On the Spatial Configuration of Scatterers for Given Delay-Angle Distributions

Alireza Borhani and Matthias Pätzold

Abstract—**This paper investigates the distribution of scatterers located around the mobile station (MS) for given delay-angle distributions. The delay-angle distribution function represents the joint probability density function (PDF) of the time-of-arrival (TOA) and angle-of-arrival (AOA). Given such a joint PDF, we first derive a general expression for the distribution of the scatterers in both polar and Cartesian coordinates. We then analyze an important special case in which the TOA and the AOA follow the multiple negative exponential (MNE) and the uniform distributions, respectively. The considered MNE PDF is the sum of several decaying exponential functions, which allows us to describe the TOA in a variety of propagation environments. For the delay profiles specified in COST 207, the scatterer distribution is simulated and visualized in scatter diagrams. The marginal PDF of the distance from the scatterers to the MS is also computed, illustrated, and confirmed by simulations. For the MNE TOA PDF, it is shown that the local scatterers are not symmetrically distributed around the MS even if the AOAs are uniformly distributed. In addition, the obtained scattering area is not confined by firm geometric constraints, which complies with real propagation environments. The importance of the work is to provide a novel approach to channel modelling, in which obtaining the desirable TOA (AOA) PDF is assured.**

Index terms — **Channel modelling, spatial configuration, scatterer distribution, scatter diagram, delay-angle distribution, multiple negative exponential.**

I. INTRODUCTION

IN the area of channel modelling, the distribution of scatterers is of crucial importance, as it allows us to study the statistical properties of the received multipath signal, such as the AOA and TOA distributions. These functions are essential for determining other characteristic quantities of the channel, like the Doppler spread, average delay, and delay spread. The spatial configuration of scatterers also plays a key role in the characterization of non-stationary channel models [1]–[4]. A variety of scatterer distributions have been proposed in the literature (see [5] and [6]). Among them, the unified disk scattering [6], uniform elliptical [7]–[9], and the Gaussian scatterer distribution model [10]–[14] are the most flexible ones, since they describe various propagation mediums with respect to the TOA and the angle-of-departure distributions [6].

According to the literature, the conventional approach to develop a new geometric-based channel model is to start from a given scatterer distribution and then to derive the statistical properties of the channel model, such as the AOA and TOA PDFs. To validate the proposed channel model, the obtained PDFs must then be validated by empirical data collected from measured channels. A good match, however, cannot always be found due to the restrictions of the proposed scattering model. As an example, many measurement campaigns (see, e.g., [15]–[17]) and specified channel models (see, e.g., [18]) show that the TOA PDF often follows a sum of negative exponential functions (acronymed by MNE TOA PDF). However, none of the scattering models studied in [5] and [6] results exactly in an MNE TOA PDF. The same disagreement might also arise by comparing measured AOA PDFs and the ones obtained from predefined scattering models.

To cope with this issue, we propose a new approach to design channel models, in which obtaining the desired TOA (AOA) PDF is incontrovertible. The starting point of our approach is not a predefined scattering model. Instead, we start from a given joint PDF of the TOA and AOA, from which the distribution of the local scatterers is derived. The given joint (marginal) PDF of the TOA and AOA can originate from either measured channels or channel specifications. In this way, we develop a channel model in which a perfect match is guaranteed between the statistical properties of the channel model and those of the measured (specified) channels. In addition, the obtained scattering area is not confined by firm geometric constraints.

Given the joint PDF of the TOA and AOA, we derive a mathematical representation for the scatterer distribution in both polar and Cartesian coordinates. As an exemplary application, the MNE TOA PDF specified in COST 207 is employed to derive the distribution of the local scatterers on the assumption that the AOA is uniformly distributed around the MS and independent of the TOA. The distribution of the scatterers in the propagation area is then illustrated in scatter diagrams. Moreover, the marginal PDF of the distance from the scatterers to the MS is derived, displayed, and compared with simulation results. An excellent agreement between the analytical and simulation results is observed. It is shown that for the MNE TOA PDF, the local scatterers are not symmetrically distributed around the MS. Notice that circularly symmetric scattering models have often been proposed in the literature (see [5] and [6]).

The rest of this paper is organized as follows. Section II is devoted to the mathematical description of the problem, whereas its general and specific solutions are provided in Section III. The simulation results are illustrated and discussed in Section IV. Finally, the conclusions are drawn in Section V.

II. PROBLEM DESCRIPTION

Fig. 1 demonstrates a typical propagation scenario with some local scatterers. Each plane wave arrives at the MS after a single-bounce caused by one of the scatterers. It is assumed that the base station (BS) acts as the transmitter, while the

A. Borhani is with the Faculty of Engineering and Science, University of Agder, 4898 Grimstad, Norway (e-mail: alireza.borhani@uia.no).

M. Pätzold is with the Faculty of Engineering and Science, University of Agder, 4898 Grimstad, Norway (e-mail: matthias.paetzold@uia.no).

MS serves as the receiver. Furthermore, we assume that both the BS and the MS are equipped with single omnidirectional antennas. The position of each scatterer can be described by polar coordinates (r, α^R), where r denotes the distance of the scatterer from the MS, and α^R stands for the AOA seen at the MS.

With reference to Fig. 1, the total path length that an emitted plane wave travels from the BS via a scatterer to the MS equals

$$D_s = r + \sqrt{r^2 + D^2 + 2rD\cos(\alpha^R)}. \quad (1)$$

The TOA τ' at the MS equals $\tau' = D_s/c_0$, where c_0 represents the speed of light. Owing to the random nature of propagation environments, the TOA τ' is a random variable, whose distribution $p_{\tau'}(\tau')$ depends on the environment. The same statement holds for the AOA α^R described by the PDF $p_{\alpha^R}(\alpha^R)$. It is worth mentioning that τ' and α^R can often be considered as independent random variables, as a certain mathematical relation between the two does not exist in most of the real propagation scenarios.

Given the joint PDF $p_{\tau'\alpha^R}(\tau', \alpha^R)$ of τ' and α^R, we are interested in finding the joint PDF $p_{r\alpha^R}(r, \alpha^R)$ of the radius r and the AOA α^R. Notice that the joint PDF $p_{r\alpha^R}(r, \alpha^R)$ represents the distribution of scatterers in polar coordinates, which is the first concern of this paper. Providing the Cartesian representation $p_{xy}(x, y)$ of the scatterer distribution is also of interest, as it allows us to visualize the scattering area in the 2D plane. In what follows, we fulfil the main objectives of this paper by deriving $p_{r\alpha^R}(r, \alpha^R)$ and $p_{xy}(x, y)$.

III. Problem Solutions

In this section, we first provide a general solution for the problem stated in Section II. Subsequently, a specific solution is presented under the assumptions of the MNE TOA PDF and the uniformly distributed AOAs.

A. General Solutions

By solving (1) with respect to r, we obtain

$$r(\tau', \alpha^R) = \frac{(\tau' c_0)^2 - D^2}{2(\tau' c_0 + D\cos(\alpha^R))}. \quad (2)$$

In the equation above, the radius r is a function of the random variables τ' and α^R. Besides this function, the auxiliary function $A(\tau', \alpha^R) = \alpha^R$ is beneficial, allowing us to derive the joint PDF of the radius r and the AOA α^R. It can be shown that the roots of these functions are given by

$$\tau' = c_0^{-1}\left(r + \sqrt{r^2 + D^2 + 2rD\cos(\alpha^R)}\right) \text{ and } \alpha^R = A. \quad (3)$$

By applying the concept of transformation of two random variables [19, p. 130], the joint PDF $p_{r\alpha^R}(r, \alpha^R)$ of r and α^R is given by the following expression

$$p_{r\alpha^R}(r, \alpha^R) = |J|^{-1} \times p_{\tau'\alpha^R}\left(c_0^{-1}(r + \sqrt{r^2 + D^2 + 2rD\cos(\alpha^R)}), \alpha^R\right) \quad (4)$$

in which $|J|$ stands for the Jacobian of the transformation. This quantity can be obtained by computing the following determinant

$$|J| = \left|\begin{matrix} \frac{\partial \tau'}{\partial r} & \frac{\partial \tau'}{\partial \alpha^R} \\ \frac{\partial \alpha^R}{\partial r} & \frac{\partial \alpha^R}{\partial \alpha^R} \end{matrix}\right|^{-1} = c_0 \left|1 + \frac{r + D\cos(\alpha^R)}{\sqrt{r^2 + D^2 + 2rD\cos(\alpha^R)}}\right|^{-1}. \quad (5)$$

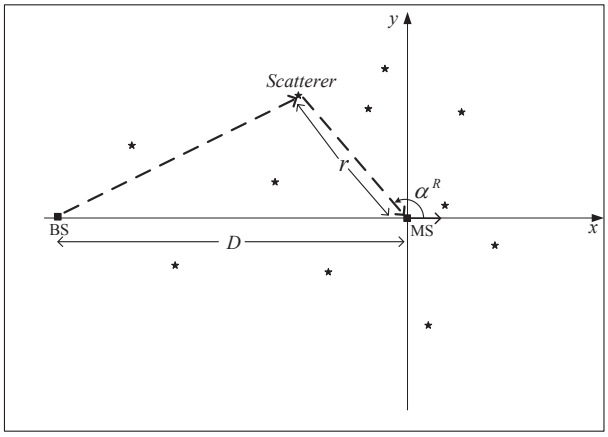

Fig. 1. A typical multipath propagation scenario with some local scatterers ($\star$).

To derive the Cartesian representation $p_{xy}(x, y)$ of the scatterer distribution from its polar representation in (4), we use the following transformations $x = r\cos(\alpha^R)$ and $y = r\sin(\alpha^R)$. Applying again the concept of transformation of random variables, we obtain

$$p_{xy}(x,y) = c_0^{-1}\left|\frac{1}{\sqrt{x^2+y^2}} + \frac{1 + \frac{Dx}{x^2+y^2}}{\sqrt{(x+D)^2+y^2}}\right| \times p_{\tau'\alpha^R}\left(c_0^{-1}(\sqrt{x^2+y^2} + \sqrt{(x+D)^2+y^2}), \arctan\left(\frac{y}{x}\right)\right). \quad (6)$$

An important special case occurs if the TOA τ' and the AOA α^R are independent random variables. In this case, the joint PDF $p_{\tau'\alpha^R}(\cdot, \cdot)$ in (4) (or equivalently (6)) can be represented as the product of the marginal PDFs $p_{\tau'}(\cdot)$ and $p_{\alpha^R}(\cdot)$. These marginal PDFs can be obtained either from measured channels (see, e.g., [15]–[17]) or from specified channel models (see, e.g., COST 207 final report [18]).

The obtained PDF in (4) (or equivalently (6)) provides the statistical description of the scattering area from which obtaining $p_{\tau'\alpha^R}(\tau', \alpha^R)$ is assured. A remarkable feature of the proposed approach is that the obtained scattering area is not confined by geometric constraints (see (6) or (4)). However, most of the geometric channel models proposed in the literature are restricted by tight mathematical boundaries, which might spoil the performance of the overall system.

B. Specific Solutions

One of the widely addressed TOA PDFs is the negative exponential distribution function, which has been confirmed by many measurement campaigns [15]–[17]. Furthermore, the COST 207 working group developed specifications for the delay distribution in different propagation areas, showing that the delay distribution can be formulated by one or two decaying exponential functions. For instance, the TOA PDF $p_{\tau'}(\tau')$ of the channel model associated with a *typical urban*

area is specified by the following single negative exponential function [18]

$$p_{\tau'}(\tau') = \begin{cases} \frac{1}{1-e^{-7}} e^{\tau'/\mu s}, & \text{if } 0 \le \tau' < 7\,\mu s, \\ 0, & \text{otherwise,} \end{cases} \quad (7)$$

For the *bad (complicated) urban area*, $p_{\tau'}(\tau')$ is presented by the following two decaying exponential functions

$$p_{\tau'}(\tau') = \begin{cases} \frac{2}{3(1-e^{-5})} e^{\tau'/\mu s}, & \text{if } 0 \le \tau' < 5\,\mu s, \\ \frac{1}{3(1-e^{-5})} e^{-\tau'/\mu s+5}, & \text{if } 5\,\mu s \le \tau' < 10\,\mu s, \\ 0, & \text{otherwise.} \end{cases} \quad (8)$$

Motivated by the discussion above, we model the TOA PDF $p_{\tau'}(\tau')$ by the following sum

$$p_{\tau'}(\tau') = \sum_{i=1}^{I} a_i e^{-\lambda_i(\tau'-\tau'_{2i-2})} \times \left[u(\tau'-\tau'_{2i-2}) - u(\tau'-\tau'_{2i-1})\right] \quad (9)$$

which is called the MNE TOA PDF. In the equation above, I is the total number of exponential functions, the parameters a_i are normalizing constants to guarantee the unity area under the PDF $p_{\tau'}(\tau')$, and $u(\cdot)$ stands for the unit step function. In addition, λ_i is the decaying factor of the ith negative exponential function, which ranges from τ'_{2i-2} to τ'_{2i-1}. Accordingly, the window $u(\tau'-\tau'_{2i-2})-u(\tau'-\tau'_{2i-1})$ is the domain of the ith exponential function.

The MNE TOA PDF in (9) is very useful, as it allows us to model a variety of power delay profiles by adjusting the domain and the other parameters of each negative exponential functions. All these parameters can be attained from measured (specified) TOA PDFs. For example, the representation of $p_{\tau'}(\tau')$ in (9) is equal to the specified TOA PDFs in (7) and (8) by choosing the model parameters listed in Table I. It is also worth mentioning that typical and simple propagation areas need a small number I of the exponential functions to be explained (see (7)), whereas atypical and complicated ones require a higher number I (see (8)).

To obtain a specific solution, we also assume that the AOA is uniformly distributed between $-\pi$ and π, i.e., $p_{\alpha^R}(\alpha^R) = 1/(2\pi)$ if $\alpha^R \in (-\pi, \pi]$. It is also assumed that the AOA α^R is independent of the TOA τ', allowing us to write $p_{\tau'\alpha^R}(\tau', \alpha^R) = p_{\tau'}(\tau')p_{\alpha^R}(\alpha^R)$. Using this property and substituting (9) and $p_{\alpha^R}(\alpha^R) = 1/(2\pi)$ in (4) and (6), the polar and Cartesian representations of the scatterer distribution are given by (12) and (13), respectively [see the bottom of this page].

IV. Simulation Results

We assume that the MS is located at the origin of the Cartesian coordinates, while the BS is placed on the negative part of the x-axis at a distance of $D = 1$ km from the MS (see Fig. 1). To specify the TOA PDF presented in (9), we use the two sets of the model parameters listed in Table I, which permits us to analyze the distribution of the scatterers in typical and bad urban areas. For the two sets, we first display the corresponding joint PDF $p_{xy}(x, y)$ and then evaluate its correctness by the scatter diagrams obtained from simulation results. The marginal PDF $p_r(r)$ of the radius r is also plotted and verified by simulation results.

Fig. 2 shows the joint PDF $p_{xy}(x, y)$ (see (13)) in the logarithmic scale for a typical urban area with the delay characteristics listed in Table I. A higher density of scatterers can be observed close to the MS (but not exactly at $(0, 0)$), while this density decreases with increasing the distance from the MS. This is in agreement with the exponential distribution of the TOA in (7), in which the large values of the distribution function are associated with the delays of incoming waves from nearby scatterers, whereas the tail of the function is due to far scatterers. Referring to Fig. 2, a very low density of scatterers is observed along the BS-MS connecting line. This could be attributed to the fact that the highest value of $p_{\tau'}(\tau')$ in (7) belongs to the shortest path.

To confirm the analytical result shown in Fig. 2, we have simulated the scattering area by distributing 1000 scatterers by means of the TOA PDF in (7). The uniform distribution between $-\pi$ and π has been considered to distribute the scatterers in azimuth. The result is shown in Fig. 3. The scatter diagram complies with the joint PDF $p_{xy}(x, y)$ shown in Fig. 2, as the scatterers are distributed in the same manner in both figures. Moreover, Fig. 3 shows that this propagation area might be approximated by a disk centred on a point on the BS-MS connecting line, within which the local scatterers are non-uniformly distributed. This geometry originates from the statistical properties of the channel, but not from imposed geometric restrictions. It is also noteworthy that the BS-MS connecting line is almost free of the scatterers, which meets the result presented in Fig. 2.

Fig. 4 illustrates the joint PDF $p_{xy}(x, y)$ in (13) for the bad urban channel specified by the model parameters in the last row of Table I, which result in the piecewise TOA PDF $p_{\tau'}(\tau')$ in (8). To highlight the impact of this piecewise function on the joint PDF $p_{xy}(x, y)$, we have used two different colours in Fig. 4. The darker (lighter) colour shows the density of the scatters associated with the first (second)

$$p_{r\alpha^R}(r, \alpha^R) = \frac{c_0^{-1}}{2\pi}\left|1 + \frac{r + D\cos(\alpha^R)}{\sqrt{r^2 + D^2 + 2rD\cos(\alpha^R)}}\right| \sum_{i=1}^{I} a_i e^{-\lambda_i(c_0^{-1}(r+\sqrt{r^2+D^2+2rD\cos(\alpha^R)})-\tau'_{2i-2})} \times \left[u\left(c_0^{-1}(r+\sqrt{r^2+D^2+2rD\cos(\alpha^R)}) - \tau'_{2i-2}\right) - u\left(c_0^{-1}(r+\sqrt{r^2+D^2+2rD\cos(\alpha^R)}) - \tau'_{2i-1}\right)\right] \quad (12)$$

$$p_{xy}(x, y) = \frac{c_0^{-1}}{2\pi}\left|\frac{1}{\sqrt{x^2+y^2}} + \frac{1 + \frac{Dx}{x^2+y^2}}{\sqrt{(x+D)^2+y^2}}\right| \sum_{i=1}^{I} a_i e^{-\lambda_i(c_0^{-1}(\sqrt{x^2+y^2}+\sqrt{(x+D)^2+y^2})-\tau'_{2i-2})} \times \left[u\left(c_0^{-1}(\sqrt{x^2+y^2}+\sqrt{(x+D)^2+y^2}) - \tau'_{2i-2}\right) - u\left(c_0^{-1}(\sqrt{x^2+y^2}+\sqrt{(x+D)^2+y^2}) - \tau'_{2i-1}\right)\right] \quad (13)$$

TABLE I
MODEL PARAMETERS ACCORDING TO THE CHANNEL SPECIFICATIONS REPORTED IN COST 207 [18].

COST 207	**Model parameters**								
channel models	I	c_1	c_2	λ_1	λ_2	τ_0'	τ_1'	τ_2'	τ_3'
Typical urban	1	1.0009	-	1	-	0 μs	7 μs	-	-
Bad urban	2	0.6712	0.3356	1	1	0 μs	5 μs	5 μs	10 μs

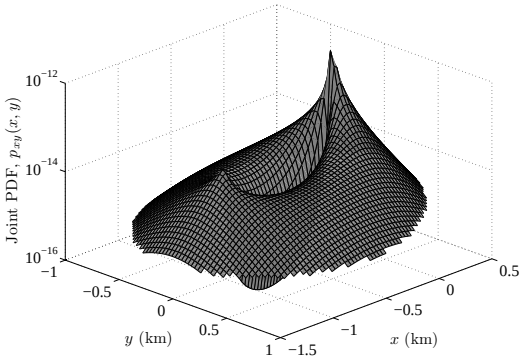

Fig. 2. The joint PDF $p_{xy}(x, y)$ (see (13)) for the typical urban channel with the TOA PDF in (7) and the uniformly distributed AOA ($D = 1$ km).

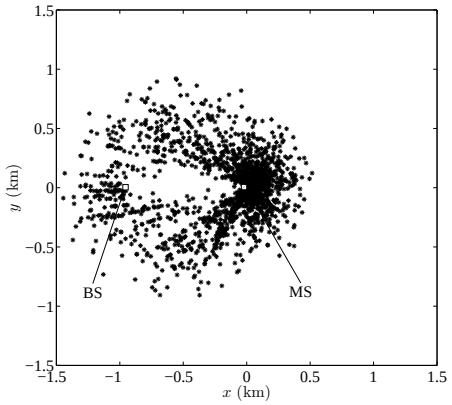

Fig. 3. The scatter diagram for the typical urban channel with the TOA PDF in (7) and uniformly distributed AOAs ($D = 1$ km).

exponential function, i.e., the one ranged from 0 to 5 μs (5 to 10 μs). Referring to this figure, the darker graph is almost like the one shown in Fig. 2, as both have been produced from almost the same delay distribution. Worth noticing is that in order to fulfill the second exponential function in (8), which is ranged from 5 to 10 μs, a larger scattering area is required. This can be observed by comparing the coverage area under the lighter and darker graphs.

Again, to validate the analytical result shown in Fig. 4, we have simulated the scattering area in such a way that the TOA PDF in (8) is satisfied. Fig. 5 shows the corresponding scatter diagram. A close agreement between the simulated scattering area and the joint PDF $p_{xy}(x, y)$ shown in Fig. 4 can be observed. By increasing the distance from the MS, the density of scatterers varies in a complicated manner. Roughly, the density first decreases, then increases rapidly, and finally decreases gradually. The extent of these variations also changes with the azimuth AOA. An unexpected high density of scatterers near the BS can also be observed. Notice that the same behaviour can also be observed in Fig. 4.

Fig. 6 demonstrates the marginal PDF $p_r(r)$ of the radius r shown in Fig. 1 for the two sets of parameters listed in Table I. This PDF can be obtained by integrating the joint PDF $p_{r\alpha^R}(r, \alpha^R)$ in (12) over the azimuth AOA α^R, i.e.,

$$p_r(r) = \int_{-\pi}^{\pi} p_{r,\alpha^R}(r, \alpha^R) d\alpha^R. \tag{10}$$

As can be seen from this figure, $p_r(r)$ decays gradually for both the typical and bad urban areas. However, for the bad urban channel model, a jump in $p_r(r)$ can be observed. An excellent match between the analytical and the simulation results can be seen. The characteristics of the plots are entirely in line with the simulated scattering areas shown in Figs. 3 and 5.

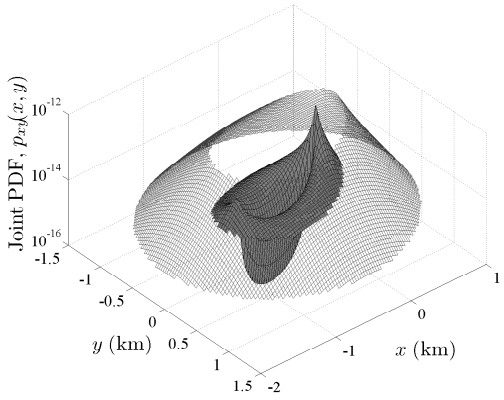

Fig. 4. The joint PDF $p_{xy}(x, y)$ (see (13)) for the bad urban channel with the TOA PDF in (8) and the uniformly distributed AOA ($D = 1$ km).

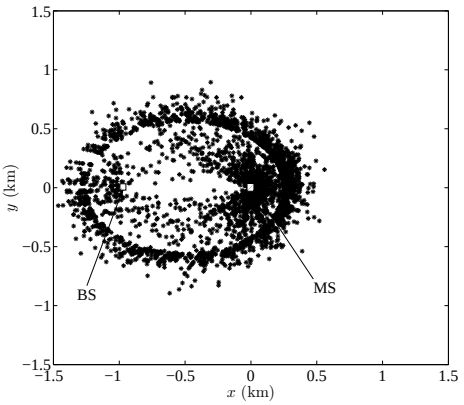

Fig. 5. The scatter diagram for the bad urban channel with the TOA PDF in (8) and uniformly distributed AOAs ($D = 1$ km).

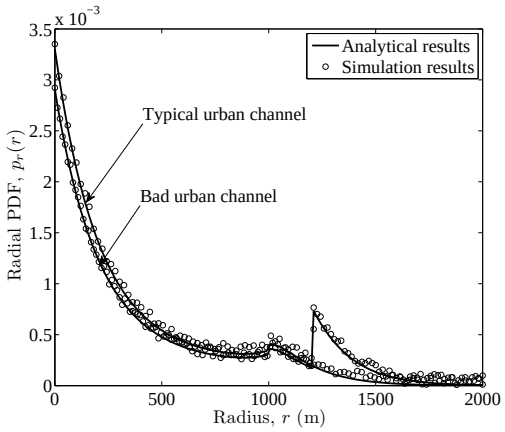

Fig. 6. The marginal PDF $p_r(r)$ (see (10)) for the typical and bad urban channels shown in Figs. 2 and 4.

V. Conclusion

In this paper, we have investigated the distribution of scatterers for given delay-angle joint PDFs. Exact analytical expressions have been provided for the polar and Cartesian representation of the scatterer distribution. The proposed approach does not impose any specific geometric constraint on the propagation area. An important special case in which the TOA follows the MNE PDF and the AOA is uniformly distributed has also been analyzed. The corresponding scattering areas have been simulated, demonstrating that a typical urban area might be modelled by a disk centred on the line between the BS and the MS. The scattering area of the bad urban channel model cannot be modelled by standard geometric shapes, as its power delay profile is mathematically complex. In such cases, the proposed approach gives a statistical representation for the scattering area. Analyzing further characteristics of the channel, such as the angle-of-departure PDF, can be investigated in future works.

References

[1] A. Borhani and M. Pätzold, "Modelling of non-stationary mobile radio channels incorporating the Brownian mobility model with drift," in *Lecture Notes in Engineering and Computer Science: World Congress on Engineering and Computer Science, WCECS'13*, vol. 2. San Francisco, USA, Oct. 2013, pp. 695–700.

[2] A. Chelli and M. Pätzold, "A non-stationary MIMO vehicle-to-vehicle channel model based on the geometrical T-junction model," in *Proc. International Conference on Wireless Communications and Signal Processing, WCSP 2009*. Nanjing, China, Nov. 2009.

[3] J. Karedal, F. Tufvesson, N. Czink, A. Paier, C. Dumard, T. Zemen, C. F. Mecklenbräuker, and A. F. Molisch, "A geometry-based stochastic MIMO model for vehicle-to-vehicle communications," *IEEE Trans. Wireless Commun.*, vol. 8, no. 7, pp. 3646–3657, Jul. 2009.

[4] A. F. Molisch, A. Kuchar, J. Laurila, K. Hugl, and R. Schmalenberger, "Geometry-based directional model for mobile radio channelsprinciples and implementation," *European Transactions on Telecommunications*, vol. 14, no. 4, pp. 351–359, 2003.

[5] K. T. Wong, Y. I. Wu, and M. Abdulla, "Landmobile radiowave multipaths' DOA-distribution: Assessing geometric models by the open literature's empirical datasets," *IEEE Trans. Antennas Propag.*, vol. 58, no. 2, pp. 946–958, Feb. 2010.

[6] A. Borhani and M. Pätzold, "A unified disk scattering model and its angle-of-departure and time-of-arrival statistics," *IEEE Trans. Veh. Technol.*, vol. 62, no. 2, pp. 473–485, Feb. 2013.

[7] I. Jaafar, H. Boujemaa, and M. Siala, "Angle and time of arrival statistics for hollow-disc and elliptical scattering models," in *Proc. 2nd Int. Conf. Signals, Circuits Syst., Nov. 2008*, pp. 1–4.

[8] R. J. Piechocki, G. V. Tsoulos, and J. P. McGeehan, "Simple general formula for PDF of angle of arrival in large cell operational environments," *Electron. Lett.*, vol. 34, no. 18, pp. 1784–1785, Sep. 1998.

[9] R. B. Ertel and J. H. Reed, "Angle and time of arrival statistics for circular and elliptical scattering models," *IEEE J. Select. Areas Commun.*, vol. 17, no. 11, pp. 1829–1840, Nov. 1999.

[10] R. Janaswamy, "Angle and time of arrival statistics for Gaussian scatter density model," *IEEE Trans. Wireless Commun.*, vol. 1, no. 3, pp. 488–497, Jul. 2002.

[11] A. Andrade and D. Covarrubias, "Radio channel spatial propagation model for mobile 3G in smart antenna system," *IEICE Trans. Commun.*, vol. E86-B, no. 1, pp. 213–220, Jan. 2003.

[12] D. D. N. Bevan, V. T. Ermolayev, A. G. Flaksman, and I. M. Averin, "Gaussian channel model for mobile multipath environment," *EURASIP J. Appl. Signal Proc.*, vol. 2004, no. 9, pp. 1321–1329.

[13] S.-H. Kong, "TOA and AOD statistics for down link Gaussian scatterer distribution model," *IEEE Trans. Wireless Commun.*, vol. 8, no. 5, pp. 2609–2617, May 2009.

[14] A. H. Kazmi and N. M. Khan, "Effect of scattering around BS on the spatial statistics of mobile channel in macrocell environment," in *International Conference on Information and Emerging Technologies (ICIET), Karachi*, vol. 1, Jun. 2010, pp. 1–5.

[15] K. I. Pedersen, P. E. Mogensen, and B. H. Fleury, "A stochastic model of the temporal and azimuthal dispersion seen at the base station in outdoor propagation environments," *IEEE Trans. Veh. Technol.*, vol. 49, no. 2, pp. 437–447, Mar. 2000.

[16] M. D. Batariere, T. K. Blankenship, and J. F. Kepler, "Wide-band MIMO impulse response measurements at 3.7 GHz," in *Proc. IEEE 45th Veh. Technol. Conf., VTC'02*, vol. 1, pp. 26–30.

[17] C. Kloch, G. Liang, J. B. Andersen, G. F. Pedersen, and H. L. Bertoni, "Comparison of measured and predicted time dispersion and direction of arrival for multipath in a small cell environment," *IEEE Trans. Antennas Propag.*, vol. 49, no. 9, pp. 1245–1263, Sep. 2001.

[18] M. Failli, Ed., *COST 207: Digital Land Mobile Radio Communications*. Luxembourg: Commission of the European Communities, 1989.

[19] A. Papoulis, *Probability, Random Variables, and Stochastic Processes*, 3rd ed. New York: McGraw-Hill, 1991.

Alireza Borhani received the B.E. degree in biomedical engineering from Azad University, Tehran, Iran, in 2007 and the M.E. degree in telecommunication engineering from Shahed University, Tehran. He is currently working toward the Ph.D. degree at the Department of Information and Communication Technology, University of Agder, Grimstad, Norway. His research interests include mobile radio communications, especially multipath fading channel modelling, multiple-input multiple-output (MIMO) systems, vehicular-to-vehicular communications, and information theory.

Matthias Pätzold received the Dipl.-Ing. and Dr.-Ing. degrees in electrical engineering from Ruhr-University Bochum, Bochum, Germany, in 1985 and 1989, respectively, and the habil. degree in communications engineering from the Technical University of Hamburg-Harburg, Germany, in 1998. From 1990 to 1992, he was with ANT Nachrichtentechnik GmbH, Backnang, Germany, where he was engaged in digital satellite communications. From 1992 to 2001, he was with the department of digital networks at the Technical University Hamburg-Harburg. Since 2001, he has been a full professor of mobile communications with the University of Agder, Norway. He authored several books and numerous technical papers. His publications received ten best paper awards. He has been actively participating in numerous conferences serving as TPC chair and TPC member.